Numerical Analysis and Design Provision Development for the Simple for Dead Load–Continuous for Live Load Steel Bridge System

REZA FARIMANI, SAEED JAVIDI, DEREK KOWALSKI and ATOROD AZIZINAMINI

ABSTRACT

The proposed connections of steel bridge girders at the pier for the simple for dead load and continuous for live load concept (SDCL) were investigated. Analytical models were developed for four connection types that previously were tested in the structural lab. For the numerical modeling of the tested specimens, nonlinear finite element was utilized. The behavior of the numerical models of each tested specimen was verified by the experimental results. The force resistance mechanism of each specimen was studied using the experimental and numerical data. In developing a resistance mechanism for the connections, the yielding of the rebar in the slab, the steel girder bottom plate and the crushing of the concrete diaphragm at pier were considered. A set of detailed equations was developed to conceptualize the connection behavior at the ultimate capacity under negative flexure. The developed equations show a good agreement with the finite element analysis results. For practical purposes, simplified equations were derived from the more detailed equations to calculate the negative ultimate flexure capacity, at the section through the pier, for two connection types. To verify the proposed design equations for a wider range of bridges, a parametric study was performed. The nonlinear finite element models of the bridges from the parametric study were used for verification of the proposed equations.

Keywords: steel bridges, steel girders, SDCL, simple for dead load–continuous for live load.

INTRODUCTION

This paper is part of series of publications describing the development and implementation of the simple for dead–continuous for live (SDCL) bridge system for steel girders. The SDCL bridge system utilizes a joint detail at the interior supports that does not become continuous until after the dead loads have been applied. Prior to attaining this final continuity, the girders within the individual spans are simply supported. General information regarding the behavior and design of the SDCL system can be found in the companion paper by Azizinamini (2014).

Four details for the connection of the girders over the pier were proposed based on preliminary studies. Full-scale specimens of these connections were tested in the lab for fatigue and ultimate loading, similar to what an actual

bridge could experience. Additional details of the testing can be found in the companion paper by Lampe et al. (2014), and complete results are contained in the project reports by Azizinamini, Lampe and Yakel (2003) and Azizinamini et al. (2005) and graduate theses by Lampe (2001), Mossahebi (2004) and Javidi (2009).

In this paper, the results of nonlinear finite element modeling of the connection details are presented. Based on the experimental data and numerical analysis, the load resistance mechanism of each connection under ultimate design loads is discussed. Design equations are then derived based on the resistance mechanism. Finally, parametric study was carried out to comprehend the sensitivity of the proposed simplified design equations.

CONNECTION DETAILS

Figure 1 shows each of the three connection details investigated. The following sections provide description of each detail.

Type 1 Connection: Bottom Flange Continuous

This class of connection represents details where bottom flanges are made continuous. The continuity in the test specimen was achieved by welding the extension of bottom flanges, as shown in Figure 1a. This detail is to represent the continuity of the compression flange. A more practical detail is where steel blocks welded to bottom flanges similar to the

Reza Farimani, Ph.D, P.E., LEED AP, Associate, Thornton Tomasetti, New York, NY. E-mail: rfarimani@thorntontomasetti.com

Saeed Javidi, Ph.D., P.Eng., Structural Engineer, Associated Engineering Ltd., Burnaby, BC, Canada. E-mail: sjavidin@gmail.com

Derek Kowalski, P.E., Design Engineer, Nucor-Vulcraft Group, Norfolk, NE. E-mail: derek.kowalski@nucor.com

Atorod Azizinamini, Ph.D., P.E., Professor and Chair, Civil and Environmental Engineering Department, Florida International University, Miami, FL (corresponding). E-mail: aazizina@fiu.edu

type 4 connection described later. The top flanges were not connected, but a rebar cage was placed in the diaphragm to connect the two girders. The continuity of the bridge girders—specifically, the ability to resist tensile forces due to live load negative moment—was provided.

Type 2 Connection: Bare End

The conceptual detail of this type is seen in Figure 1b. The second detail was similar to the first test, except that the bottom flanges were not welded, and no end plate was added to the girders. Basically, two W-shape girders were simply placed on the pier and embedded in the concrete diaphragm. Again, the tension portion of the continuity for live load was provided by continuous longitudinal rebar in the slab.

Type 3 Connection: End Plate

The third detail was similar to the first detail, except that the bottom flanges were not extended and welded, as shown in Figure 1c. End plates were installed similar to the first detail. The continuity for live load was again provided by continuous longitudinal reinforcement in the slab.

Type 4 Connection: Modular

A final detail has been developed that can be used in conjunction with bridges constructed using conventional or accelerated construction philosophy. Figure 2 shows the connection detail over the pier. In this detail, a thick plate, which is referred to as a "block" in this paper, was welded to each girder bottom flange, as seen in Figure 3. The girders were placed on the pier such that the blocks came in contact with each other but were not welded together. The continuity for live load negative moment was provided by longitudinal

slab rebar with 90° hooks in the concrete diaphragm. The development of this connection and additional details are discussed in the fifth paper of this series (Javidi, Yakel and Azizinamini, 2014).

NUMERICAL STUDY

The connections described in the previous sections were modeled by nonlinear finite element programs to study their behavior in more detail and develop information that could complement the experimental results. Two commercial finite element software packages (ANSYS 5.7 and ABAQUS 6.9) were used independently for the modeling of the test specimens. The following sections address the details of finite element analysis (FEA) using ABAQUS. Details of the numerical work conducted using ANSYS are provided elsewhere (Farimani, 2006).

Modeling

The finite element models consisted of the steel girder, concrete slab, concrete diaphragm, bearing pads and rebar and steel details such as stiffeners and shear studs. The sizes and dimensions of the elements were obtained from the specimen as-built drawings.

Material Properties for Steel

The steel material properties were acquired from coupon tests obtained from the girders, as well as rebar. The material test details and their results can be found in the research report by Azizinamini et al. (2005). In this study, a multilinear isotropic hardening material based on true stress-strain curve of the materials was considered in the modeling (Javidi, 2009).

(a)　　　　*(b)*　　　　*(c)*
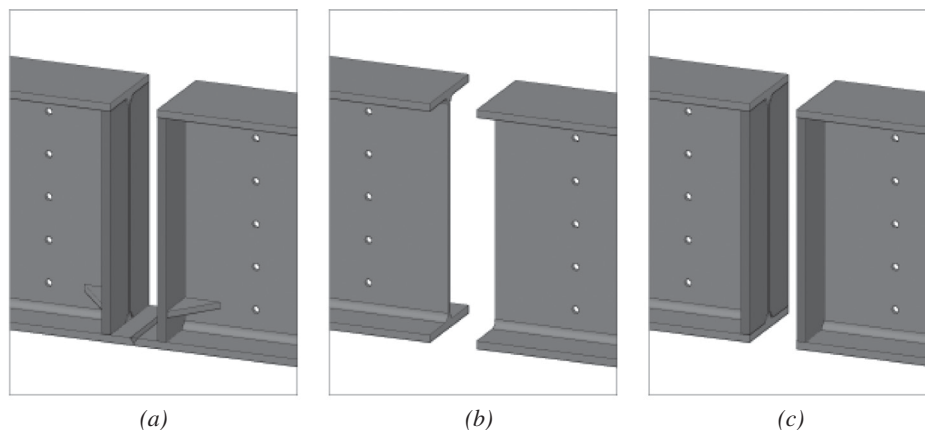
Fig. 1. Details of specimens inside the diaphragm: (a) type 1; (b) type 2; (c) type 3.

Concrete Material Modeling

The reinforced concrete was modeled using the concrete damaged plasticity model in ABAQUS. In this technique, the rebar was modeled by truss elements with compatible displacement with the concrete element around the rebar. The inelastic behavior of concrete in the concrete-damaged plasticity model is based on a concept of combined isotropic-damaged elasticity and isotropic tensile (compressive)
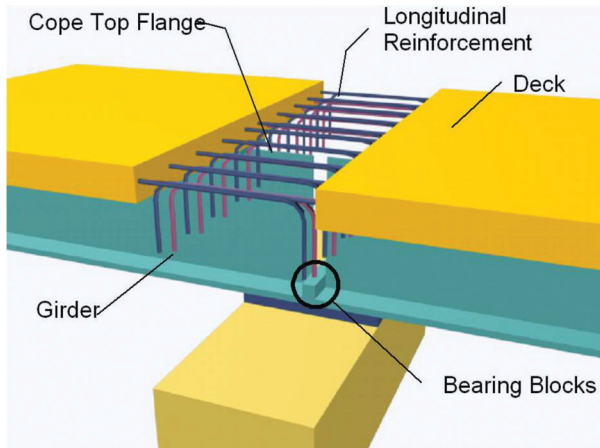
Fig. 2. *Pier connection detail for modular system (type 4).*

plasticity. Concrete in compression, based on the amount of strain, can have a linear-elastic, nonlinear-elastic and non-linear-plastic behavior.

In tension, concrete behaves as linear-elastic to the maximum tensile strength and has nonlinear post-cracking behavior. In this study, tension stiffening is applied to the model by the post-failure stress-strain relationship. Exponential behavior was chosen to describe the tension-stiffening curve after maximum tension strength of the concrete (ABAQUS, 2009).

In compression, the Carreira-Chu model (ABAQUS, 2009) was adopted in the FEA modeling of this study. In this model, the uniaxial-compression stress-strain curve is assumed to be linear up to $0.3f_c'$, where f_c' is the 28-day compressive strength of the standard cylinder, followed by a nonlinear behavior up to failure.

In multi-axial stress states, the uniaxial behavior of concrete can be generalized through the failure surface and ultimate strength in stress space. For the failure criteria of concrete, the Drucker-Prager model (ABAQUS, 2009) was adopted.

Element Type

In the finite element models, the girders, stiffener plates and end plates were modeled by a four-node, doubly curved, general-purpose, structural shell element. The shear studs, dowels and bolts were modeled using beam elements.
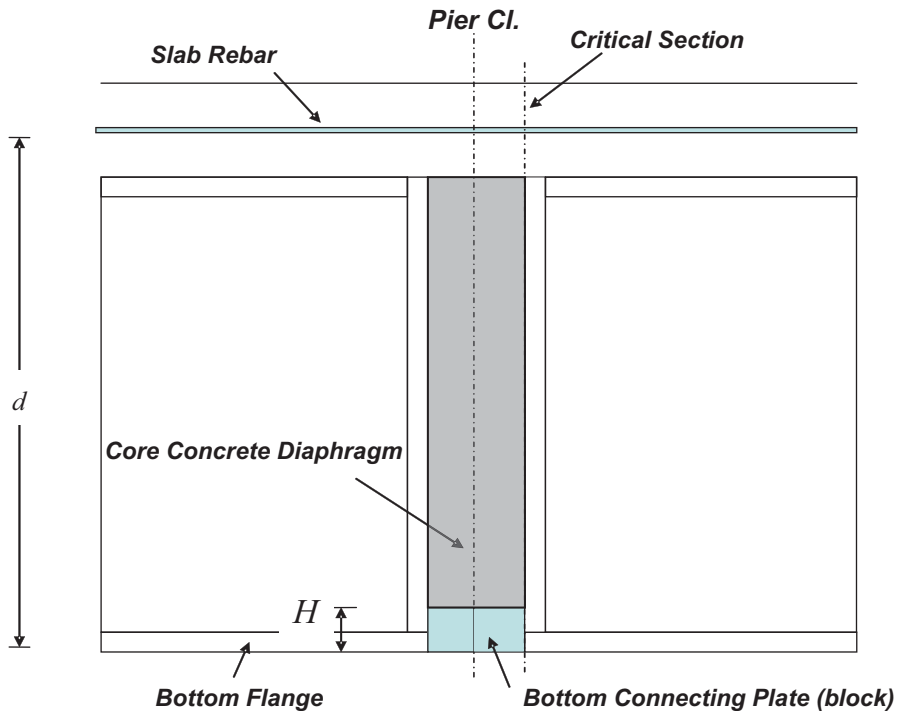
Fig. 3. *Details of specimens inside the diaphragm.*

All reinforcing bars were modeled using truss elements with only an axial degree of freedom.

Boundary Conditions and Connectivity

All reinforcing bars are embedded in concrete. The girders are connected to the deck by embedding the shear studs in the concrete deck. The elastomeric pad is constrained in all three translation directions. Two shear locks are restrained in only the transverse directions. Therefore, the bearing pad is the only element that can carry load in the vertical direction as a support.

Solution Strategy

Several sensitivity analyses were carried out to test the sensitivity of the different parameters of the model. To verify mesh size, different element sizes were employed, and the proper mesh size was selected for final analysis.

Different approaches were employed to observe the effect of the loading type. It was noticed that using a spreader beam, similar to the one used in the tests, was a better approach to model the loading. Load was applied to the specimen in a displacement-control fashion. Static analysis was chosen due to the low rate of monotonic loading applied in the tests.

Results

The following sections examine the results obtained from the finite element analyses and compare the results with those obtained from experimental testing.

Load-Displacement

Load-displacement results obtained from experimental testing and the corresponding numerical analysis of all described specimens are shown in Figures 4, 5 and 6. The notable events that a specimen experienced during loading are shown on the plots. These events consist of first cracking in the concrete, yielding of the steel and crushing of the concrete. These events were obtained from FEA results and were verified by the available experimental data.

Figure 4 shows the load displacement for the type 1 connection with a continuous bottom flange. In this specimen, the first yielding occurred in the top longitudinal reinforcement of the slab; subsequently, the bottom plate that connected the two girders yielded. In the next stage, the concrete between the two girder end bearing plates crushed. It should be noted that the crushing of the concrete was localized and in the vicinity of the compression flange. The yielding of all rebar occurred after the crushing of the concrete. The
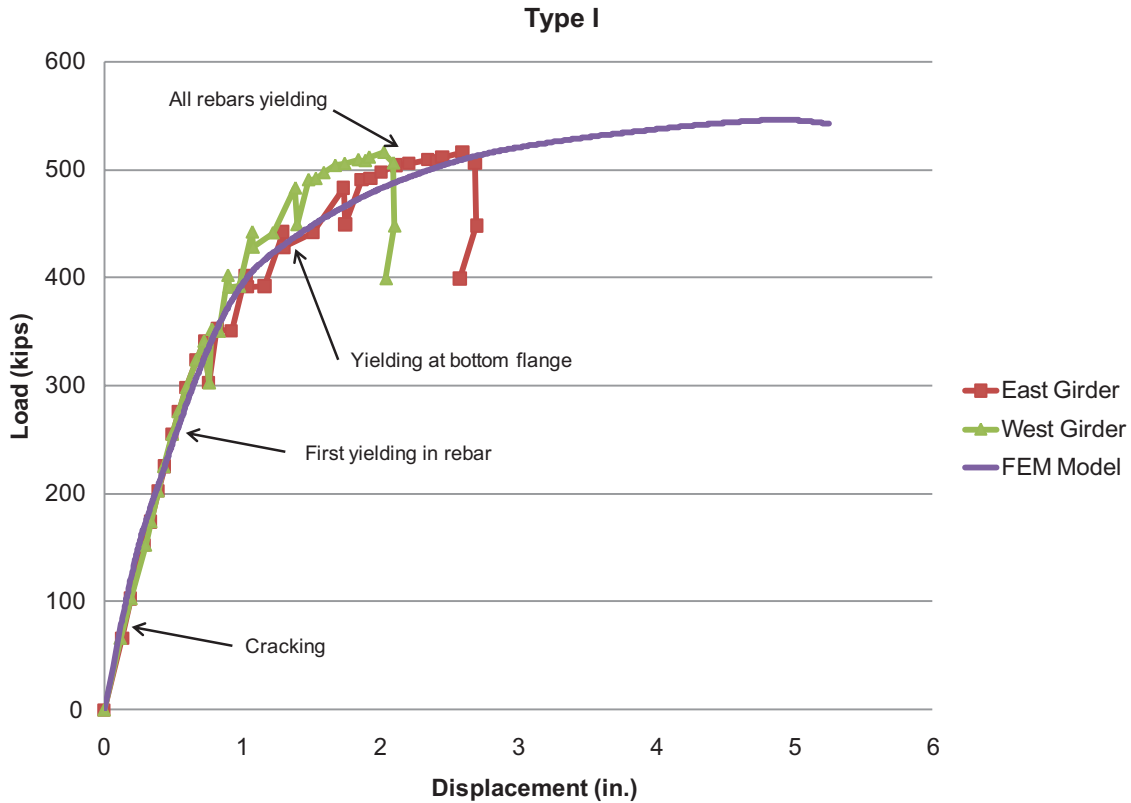
Fig. 4. Load displacement behavior— type 1 (continuous bottom flange).

mode of failure predicted using the numerical model was a flexural mode of failure, consistent with the test response, due to increasing plastic strains developed in the tension reinforcement.

The finite element analysis of the second specimen was not numerically stable because crushing of the concrete occurred in the early stages of loading. In the second specimen, crushing of the concrete occurred before yielding of the rebar. The bare-ended type 2 connection results are not addressed in this paper because of its poor performance during the fatigue and ultimate experimental tests.

Figure 5 shows the load-displacement curve of the finite element model (FEM) results versus experimental results for the type 3 connection with end plate. In the third specimen, the yielding was initiated in the top slab rebar, and crushing occurred after the partial yielding of the slab bars. The failure of the specimen occurred upon yielding of all slab reinforcements.

Figure 6 shows the load-displacement curve of the experimental test and FEM result for the modular type 4 connection. In this specimen, the top longitudinal bars yielded at the edges of the concrete diaphragm over the pier. At this location, the longitudinal rebar typically did not overlap. During the final stage of loading, all of the slab rebar yielded.

Based on the test results and the finite element studies, it was observed that there were three main modes of failure for the specimens:

1. All of the slab longitudinal rebar yielded under negative flexure. Failure of the specimen was due to the excessive plastic strain in the reinforcing bars.

2. The concrete crushed at the bottom part of the diaphragm under compression, preventing the yielding of all of the longitudinal reinforcement over the pier.

3. Some of the rebar yielded in the slab, but crushing of the concrete resulted in failure of the specimen.

Strain Distribution in Slab Longitudinal Rebar

It was observed in the tests and FEM results that the strain distribution in the top rebar across the width of the slab is not uniform. Figures 7, 8 and 9 show the strain distribution in various stages of loadings for each specimen.

The main reason for nonlinearity of strain—and, consequently stress in the slab—is the shear lag in the concrete slab.

In a vertical section along the depth of the girder, a linear distribution assumption—that is, plane sections remain
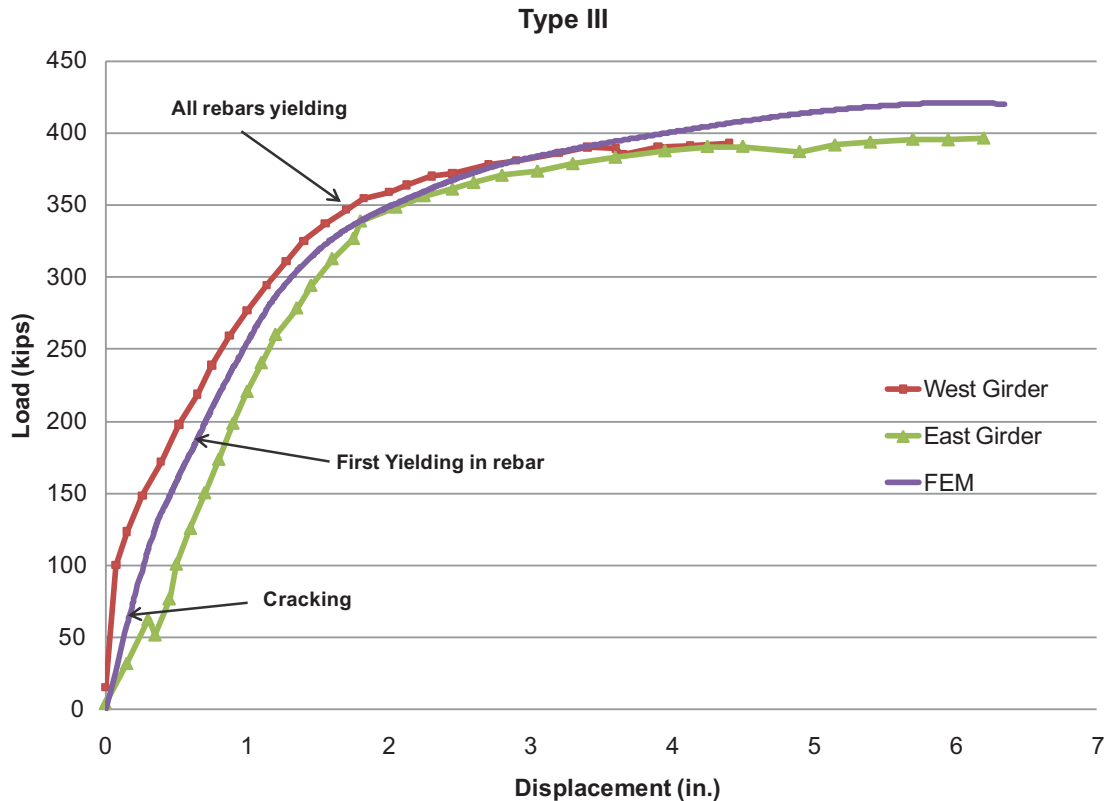
Fig. 5. Load vs. displacement—type 3 (end plate).
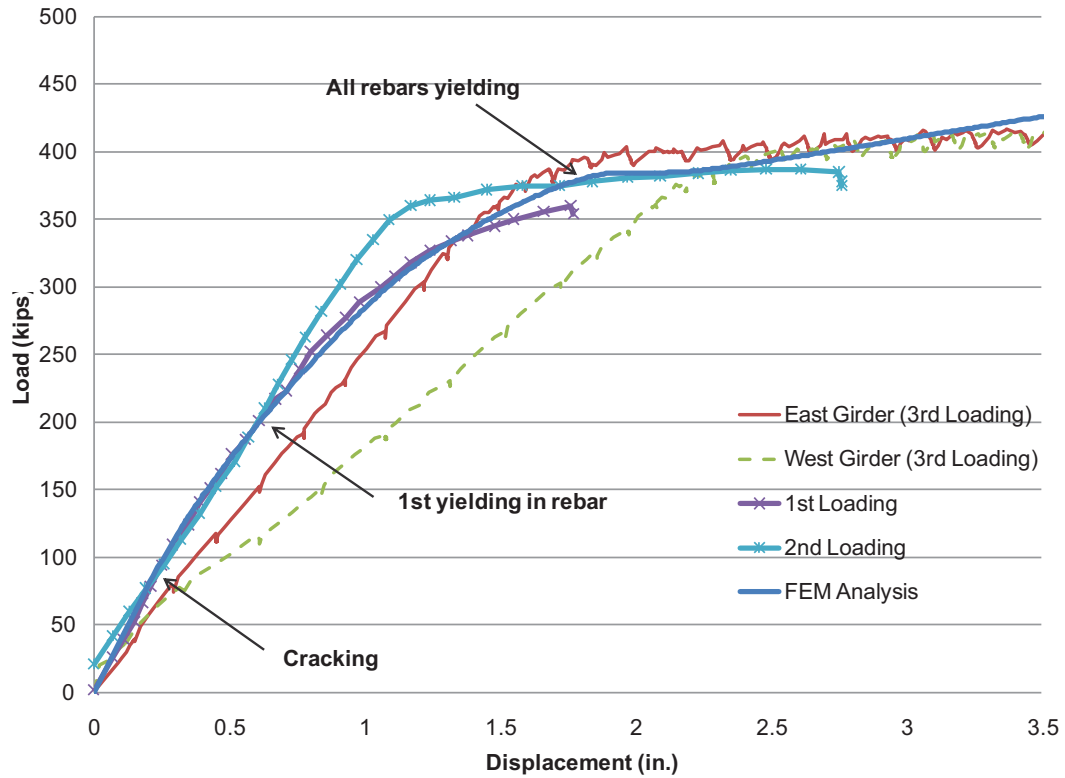
Fig. 6. Load vs. displacement—type 4 (modular).
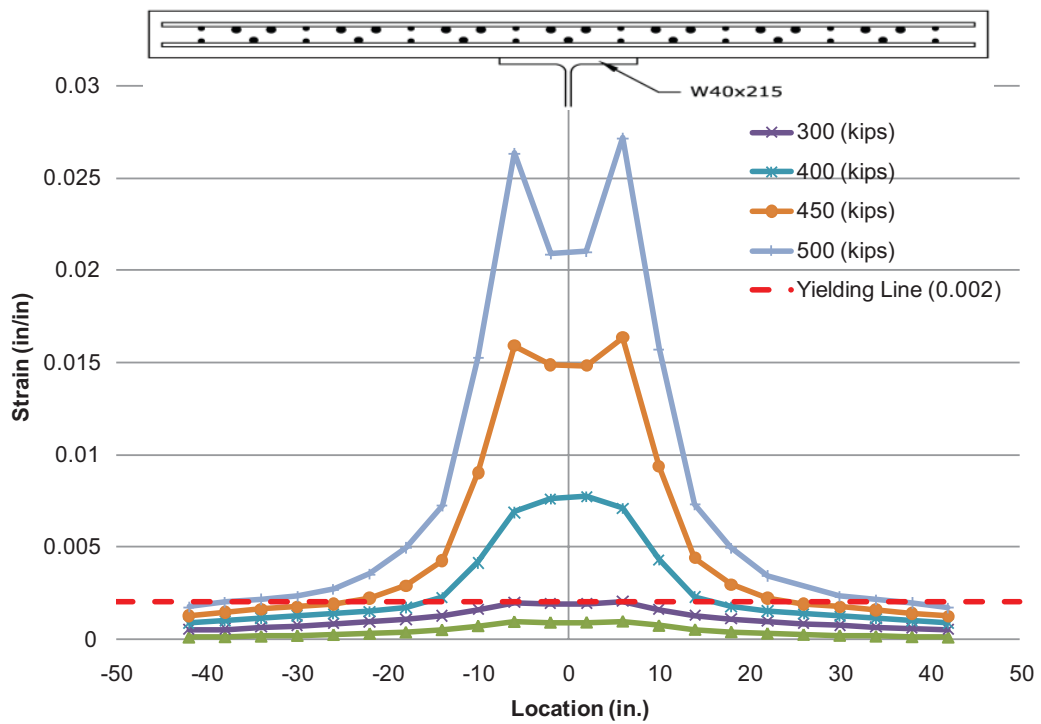
Fig. 7. Rebar strain distribution—type 1 (continuous bottom flange).
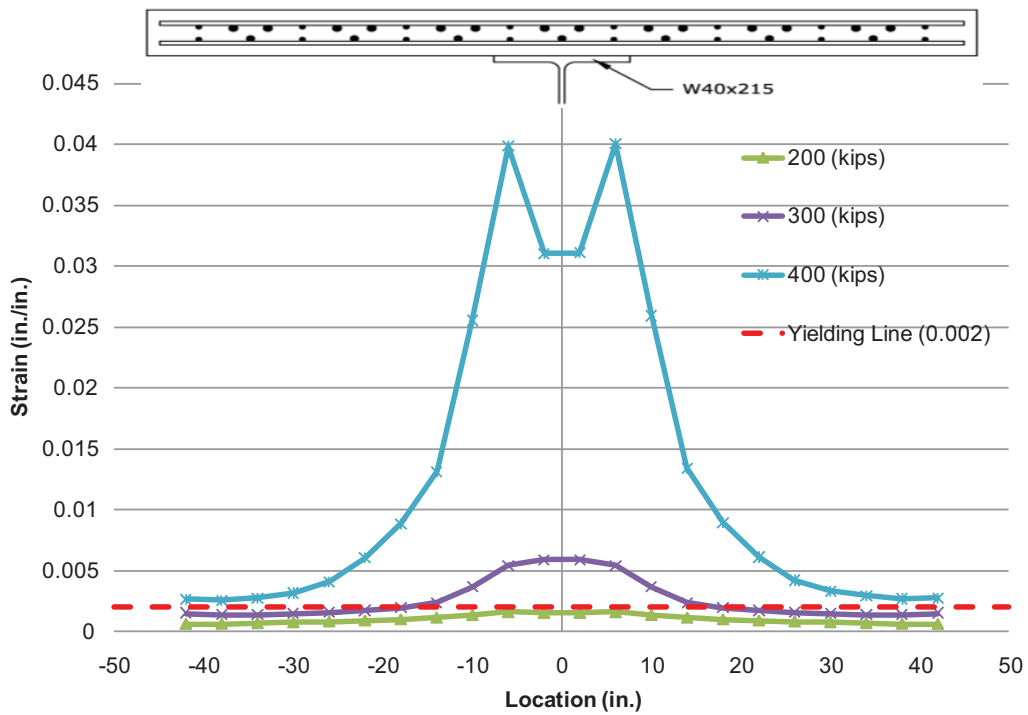
Fig. 8. Rebar strain distribution—type 3 (end plate).
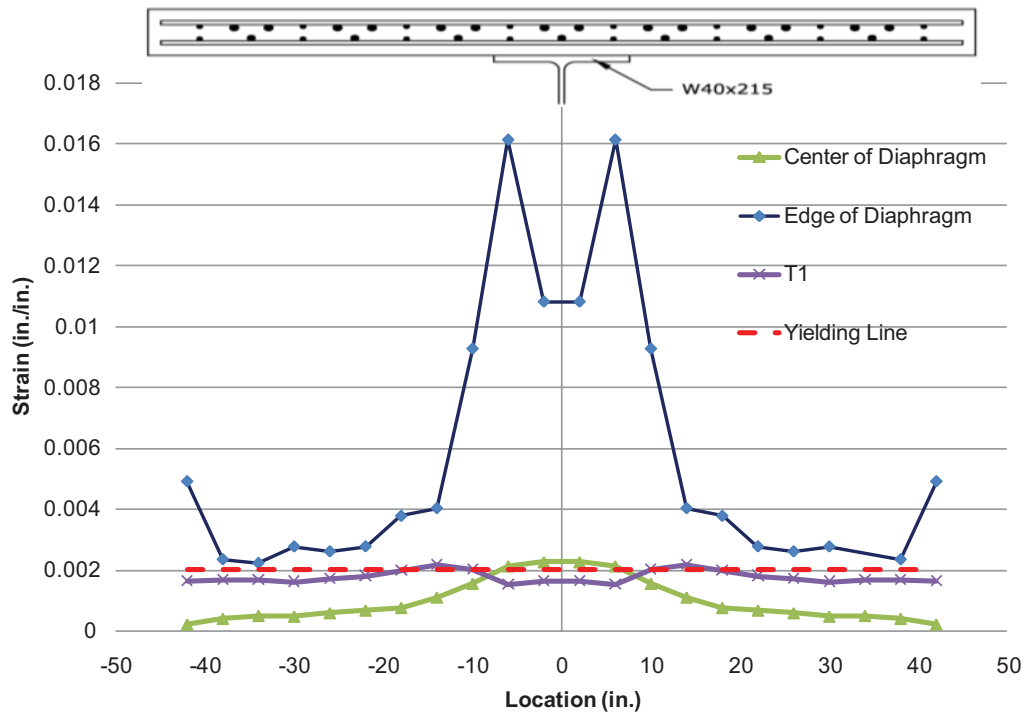
Fig. 9. Rebar strain distribution—type 4 (modular).
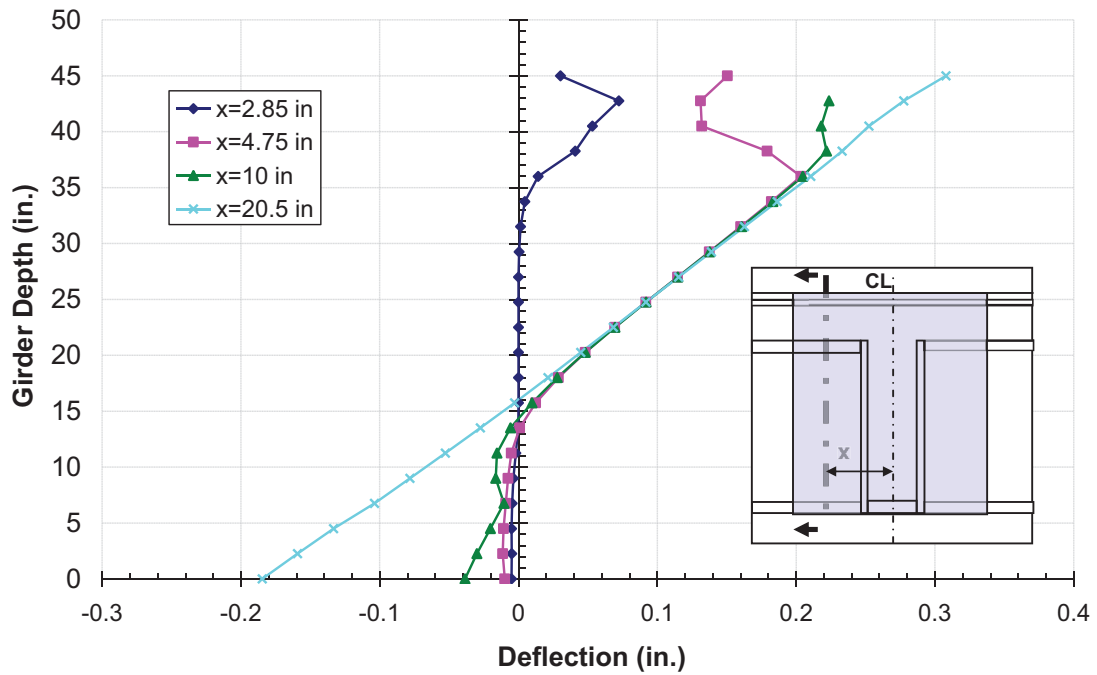
Fig. 10. Vertical strain distribution—type 1 (continuous bottom flange).
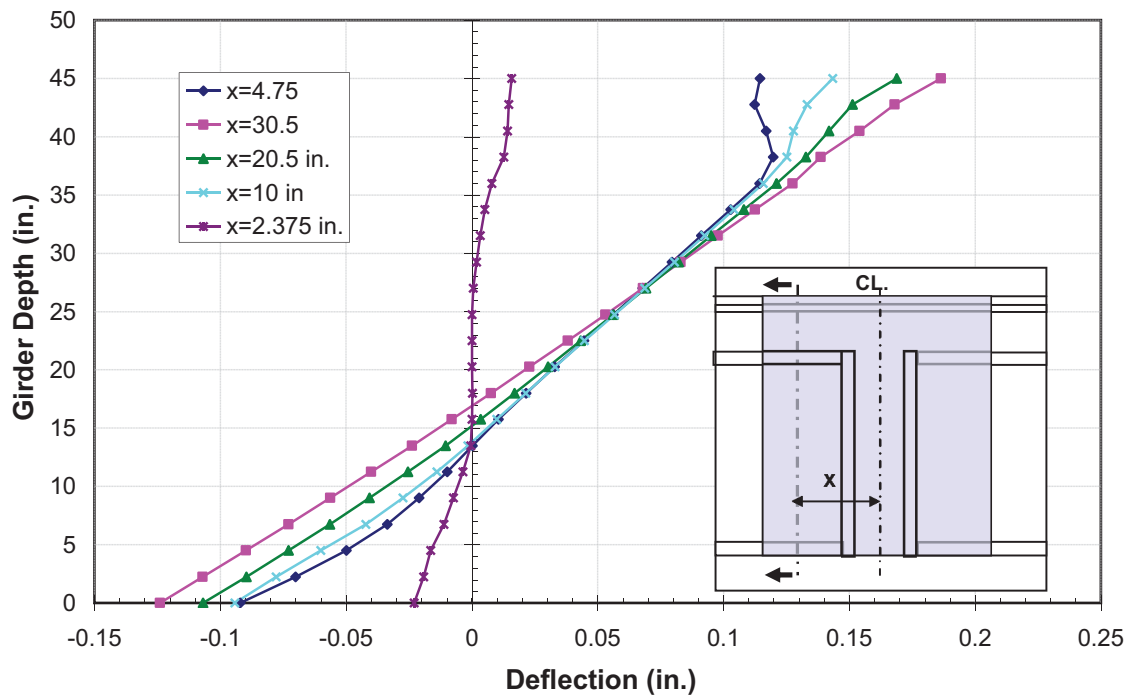
Fig. 11. Vertical strain distribution—type 3 (end plate).

plane (Bernoulli's principle)—is not valid based on the tests and finite element results. The profiles of the deflection of the sections inside the concrete diaphragms are shown in Figures 10 and 11 for the type 1 (continuous bottom flange) and type 3 (end plate) specimens, respectively. However, the strain distribution in sections farther from the pier centerline tends to be linear. This is also valid for the modular type 4 connection, as shown in Figure 12. In this figure, the strain distribution is depicted at the edge of the diaphragm. Note that for design purposes, a linear strain distribution was utilized, similar to traditional reinforced concrete design.

LOAD RESISTANCE MECHANISM BASED ON EXPERIMENTAL AND FINITE ELEMENT RESULTS

The elements that resist the applied negative moment in the concrete diaphragm are the top and bottom layers of longitudinal rebar in the slab, the concrete diaphragm in tension, the rebar hoops, the bottom plate or steel block and the concrete in compression. The results of finite element analyses indicate that the slab rebar, bottom connection plate or concrete core are the main elements contributing to the ultimate negative moment resistance of the tested connections. Other elements such as tension resistance in the concrete, diaphragm rebar hoops and the concrete diaphragm outside

of the core have less effect, which can be neglected in calculations of the ultimate moment capacity.

Idealized Stress and Strain Distributions

For the purpose of design, based on the test and FEA results, idealized strain and stress distributions are proposed for the pier centerline section at the ultimate condition.

Longitudinal Reinforcement

It is evident from both test data and finite element analysis that the stress is not uniformly distributed in the slab rebar along the slab width. This phenomenon was also demonstrated by Timoshenko and Goodier (1970) using a stress function that satisfies the two-dimensional linear elasticity differential equation, along with the boundary conditions. The main reason for nonlinearity of strain—and, consequently, stress in the slab—is the shear lag phenomenon (Timoshenko and Goodier, 1970).

To derive a strain distribution, in the longitudinal reinforcement across the slab width and for the ultimate condition similar to what was observed in the tests and FEA, a simplified model was developed. In this model, as shown in Figure 13, the slab is assumed to act as a continuous beam supported by series of longitudinal reinforcement. The longitudinal reinforcements are modeled using one-dimensional
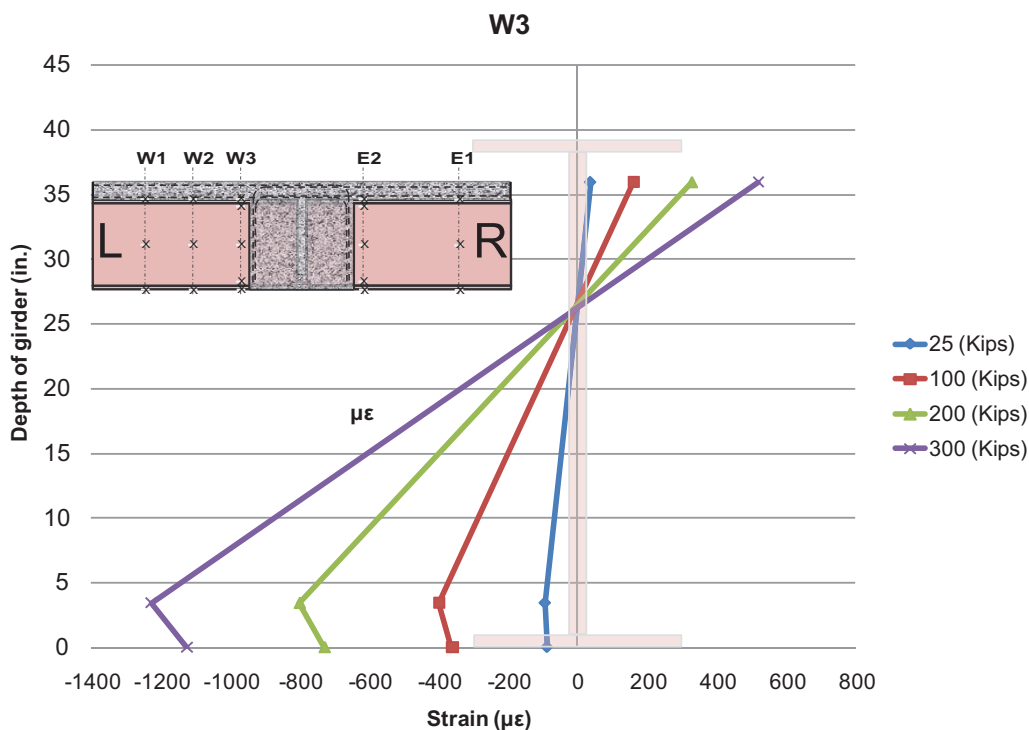
Fig. 12. Vertical strain distribution at edge of diaphragm—type 4 (modular).

springs, and the shear is transferred to the reinforcements through the concrete slab. The differential equation for a beam resting on springs is given by

$$\frac{d\delta}{dy} = -\frac{kv}{G_c A_c} \qquad (1)$$

where

δ = deflection of the beam as a function of y
k = shear stress factor, which is about 1.5 for rectangular sections
v = shear force in any section of the beam
G_c = shear modulus
$A_c = t_s\Delta$
T_s = slab thickness
Δ = crack spacing

Solving the differential equation in Equation 1 results in:

$$\varepsilon = \frac{V\lambda}{2dk_r\left(1 - e^{\frac{-\lambda b_s}{2}}\right)} e^{-\lambda y} \qquad (2)$$

Or, in a simpler form,

$$\varepsilon = \varepsilon_s e^{-\lambda y} \qquad (3)$$

where

$$\lambda = \sqrt{\frac{1.5k_r}{0.4G_c A_c}}$$

L = length of the cantilever girder
V = shear force
d = distance between the center of the slab reinforcements and the center of the compression force in the concrete diaphragm
k_r = slab rebar stiffness
k_s = stiffness of a strip of concrete slab
ε_s = constant
ε_y = strain of rebar at yielding

For design purposes, a uniform strain and stress distribution is assumed over the width of the top flange (b_f in Figure 14) with an exponential strain distribution everywhere else. The stress distribution follows the strain distribution in the linear region, which is exponential. It is uniform in the yielded areas (denoted by b_e in Figure 14).
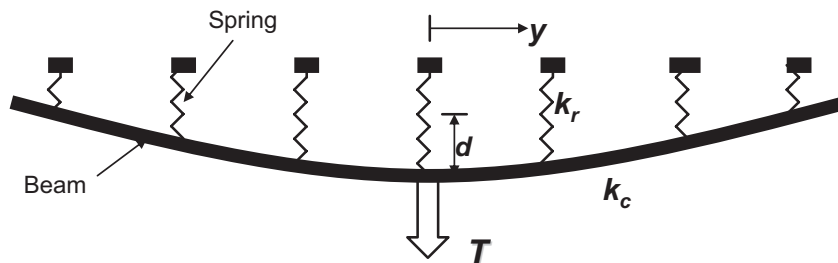
Fig. 13. Beam-spring model for a slice of the concrete slab and the rebar.
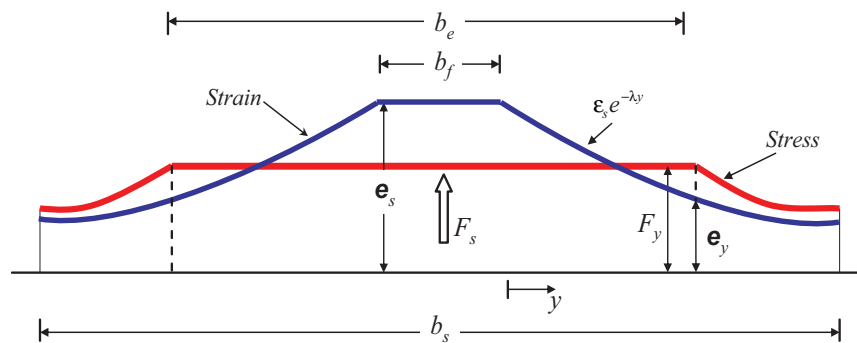
Fig. 14. Stress and strain distribution across the width of slab in reinforcement.

Diaphragm Concrete

Figure 15 shows the simplified stress and strain profiles in the concrete through the depth of the diaphragm in the middle of pier. The strain distribution is assumed to be linear, while the stress profile is nonlinear.

A uniform stress distribution is assumed for the core concrete region across the width of the end bearing plate as shown in Figure 16, and an exponential stress distribution is considered for the concrete diaphragm outside the core region.

Concrete Strength

Results of numerical studies indicate that the crushing of the concrete between the two end bearing plates (the core concrete) was the reason for failure of specimens 2 and 3 (more so for specimen 2). Based on the finite element results of the third specimen, most of the compressive force in the bottom flange of the steel girder is transferred through the core concrete. The finite element results also confirm that the compressive stress in this region is higher than the uniaxial compressive strength of the concrete due to the confinement of the core concrete by the surrounding concrete diaphragm

and the end bearing plates. A simple model was implemented to achieve a closed-form solution for the concrete strength in the triaxial stress state for design purposes. This is shown in Figure 17. The applied pressure, q, is resisted by the direct concrete compressive strength, f_c, plus shear resistance denoted by s, in Figure 17.

$$qab_f = 2sat_c + f_c ab_f \qquad (4)$$

where

a = depth of compression stress block in core region
b_f = width of the end bearing plate, which is equal to flange width in current study
t_c = thickness of concrete core

The concrete compressive strength due to the diaphragm confinement can be computed based on a linear approximation of a three-parameter method developed by Willam and Warnke (1975). For a linear approximation of the failure surface, the lateral stress, shown by p in Figure 17, is assumed to be less than 20% of the normal stress, which is a reasonable assumption based on the fact that concrete cracks in this direction and the cracking stress of concrete is less
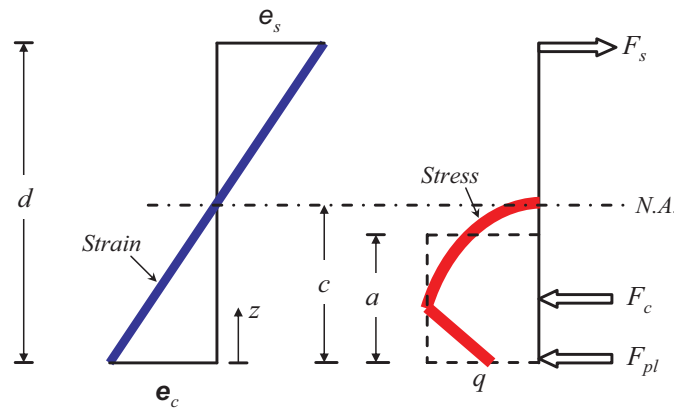
Fig. 15. Strain, stress and force diagrams in the vertical direction at the centerline of pier located in the plane of the web.
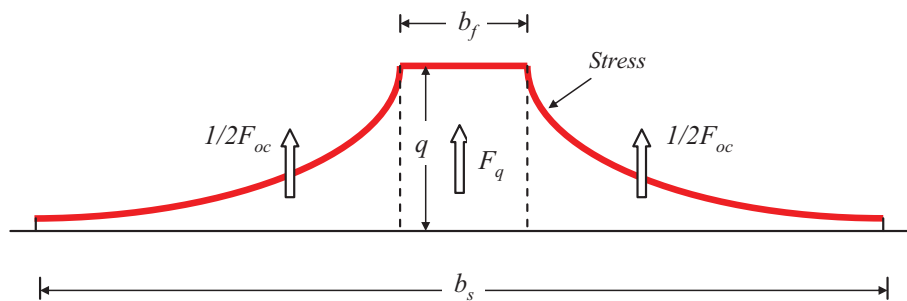
Fig. 16. Stress distribution of the compressive concrete across the width of diaphragm.

than 20% of the compressive stress. Based on a linear fit of the failure surface (Farimani, 2006), the relationship of normal stress, f_c, and lateral principal stress, p, can be described in the following formula:

$$f_c = 1.6p + f'_c \qquad (5)$$

The finite element analysis of the tested specimens indicates that the first principal stress in the core concrete region is not more than the tensile strength of the concrete. The tensile strength is adopted from the AASHTO LRFD (2007) formula for the splitting tensile strength in ksi:

$$f'_t = 0.24\sqrt{f'_c} \qquad (6)$$

Substituting from Equation 6 for p in Equation 5 gives

$$f_c = 0.38\sqrt{f'_c} + f'_c \qquad (7)$$

Shear strength, s, is conservatively taken as zero.

$$s = 0 \qquad (8)$$

Substituting Equations 8 and 7 into Equation 4, the following relationship is derived for the concrete strength in the core region:

$$q = 0.38\sqrt{f'_c} + f'_c \qquad (9)$$

where
 f'_c = uniaxial compressive strength of the concrete, ksi

The compressive strength of the core region, F_q, is computed using an equivalent rectangular stress block as shown in Figure 15:

$$F_q = qab_f \qquad (10)$$

This load is assumed to be applied at a depth equal to half of the stress block depth, a. By neglecting concrete resistance outside the core, the total compressive resistance, F_c, provided by the concrete diaphragm at the ultimate condition at the pier centerline is:

$$F_c = F_q \qquad (11)$$

Reinforcement Strength

When all of the slab rebar are in the elastic range, a linear strain-stress relationship is adopted, and the total tensile force in the slab rebar, F_s, can be computed according to the strain and stress distribution shown in Figure 14 as:

$$F_s = E_s \varepsilon_s A_s \frac{b_f}{b_s} + 2 \int_0^{\left(\frac{b_s - b_f}{2}\right)} E_s \varepsilon_s e^{-\lambda y} \frac{A_s}{b_s} dy \qquad (12)$$

In Equation 12, the origin of the y-coordinate axis has been shifted to the edge of the flange for the sake of simplicity, as seen in Figure 14. Simplifying Equation 12 gives:

$$F_s = \rho b_f + 2\frac{\rho}{\lambda}\left[1 - e^{\frac{-\lambda(b_s - b_f)}{2}}\right] \qquad (13)$$
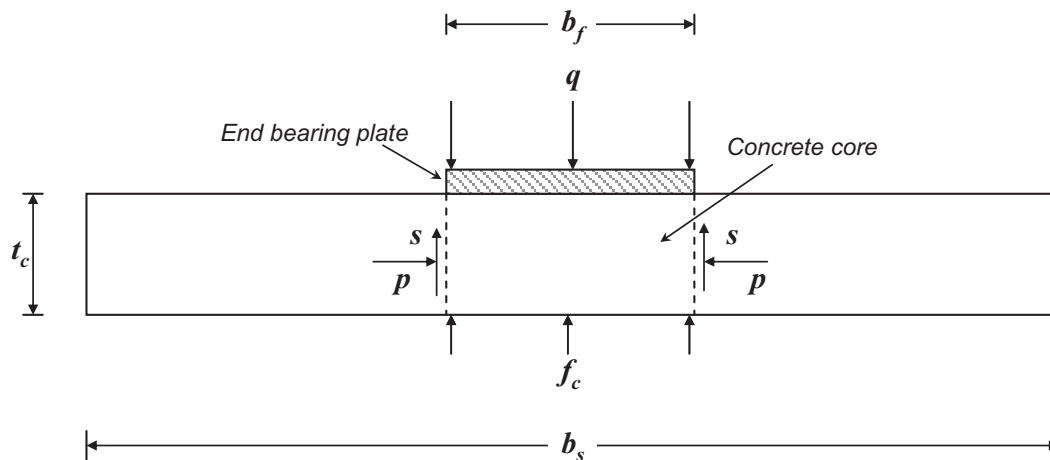
Fig. 17. End bearing plate resting on the core concrete.

Table 1. Comparison of Results of the FEA and Developed Equations					
		Specimen 1		Specimen 3	
Output	Units	Equations	FEA	Equations	FEA
F_{pl}	kips	924.30	913.0	0.00	0.00
q	ksi	7.2	6.97	6.81	7.49
F_s	kips	1474.40	1476.0	1416.20	1396.0
F_{st}*	kips	182.40	247.0	175.20	168.0
a	in.	3.8	7.06	12.2	9.79
b_e	in.	93.00	93.00	93.00	93.00
M_u	kip-in.	68061	68949	57528	61107
*F_{st} is the contribution of the stirrups in the diaphragm.					

where

$$\rho = \frac{E_s \varepsilon_s A_s}{b_s}$$

E_s = steel rebar elasticity modulus

Part of the rebar in the concrete slab might yield at the ultimate condition; in this case, the width of the yielded area (denoted by b_e as shown in Figure 14) is given by:

$$b_e = \frac{-2}{\lambda} \ln \frac{\varepsilon_y}{\varepsilon_s} + b_f \qquad (14)$$

where ε_y is the yield strain of the rebar.

The total tensile force in the rebar is computed based on the following equation:

$$F_s = \frac{b_e}{b_s} A_s F_{yr} + \frac{2E_s \varepsilon_s A_s e^{\frac{\lambda b_f}{2}}}{\lambda b_s} \left(e^{\frac{-\lambda b_e}{2}} - e^{\frac{-\lambda b_s}{2}} \right) \qquad (15)$$

where F_{yr} is the yield strength of the slab rebar.

Connecting Plate Strength

In connections similar to the first test specimen, a plate that connects two girders' bottom plates participates in transferring the compression along with the concrete. The experimental data and finite element simulations both indicate this plate yielded almost uniformly across its width. Therefore, its resistance, F_{pl} (see Figure 15), can be easily computed as follows:

$$F_{pl} = A_{pl} E_s \varepsilon_c \quad \text{if} \quad \varepsilon_c \le \varepsilon_y \qquad (16)$$

$$F_{pl} = A_{pl} F_{yp} \quad \text{if} \quad \varepsilon_c \ge \varepsilon_y \qquad (17)$$

where
A_{pl} = the cross-section area of the connecting plate
F_{yp} = yield strength of the plate
ε_c = concrete strain at the plate elevation

Verification of Proposed Mechanistic Model

The derived equations were implemented for the first and third tests to find their ultimate moment capacity at the pier. For this purpose, the depth of the concrete rectangular block, a (see Figure 15), is computed based on the force equilibrium in the section:

$$F_s - F_c - F_{pl} = 0 \qquad (18)$$

Substituting from Equations 10 and 11,

$$a = \frac{F_s - F_{pl}}{q b_f} \qquad (19)$$

The moment capacity of the section is computed based on the moment equilibrium about the center of the concrete compression block using the following equation:

$$M_u = F_s \left(d - \frac{a}{2} \right) + F_{pl} \left(\frac{a}{2} \right) \qquad (20)$$

The results are compared to the finite element analysis in the next step. It should be noted that the yield stress of the rebar was calculated based on the average stress obtained from the finite element analysis at the ultimate condition and included strain hardening effects.

The final results are listed in Table 1. The comparison of the results with the finite element analysis of the first and the third tests indicates that there is good agreement for the moment strength of these two sections.

It should be noted that the tensile strength of the stirrups was calculated in the same manner as slab rebar tensile force and added to the total force equilibrium. This was done to ensure an accurate comparison with the finite element results as listed in Table 1. Also, the tensile strength of the concrete was ignored in the design calculation listed in Table 1, but it has only a slight effect on the total flexural capacity.

SIMPLIFIED DESIGN PROVISION FOR NEGATIVE FLEXURE

In this section, the development of simplified design equations for connection types 1, 3 and 4 are addressed. These represent two classes of connections: the first class in which a bottom plate or steel block transfers the compression forces (types 1 and 4) and the second class without the bottom plate that relies on concrete to carry compressive force (type 3).

In the previous section, a detailed force transfer mechanism was developed. This detailed approach was intended to understand and comprehend the contribution of various connection elements to the load-carrying capacity. This result was used to select the important elements and develop a simplified approach that is suitable for design yet captures the essential connection behavior described in the previous section. The following assumptions were made, while developing the simplified design provisions:

- The stirrups were shown in the previous section to have a minor contribution to the strength of the connection in comparison to the other elements. Thus, they will not be considered in this section.

- Contribution of concrete in tension to moment capacity is ignored.

- The critical section for moment capacity calculation purposes is assumed to be inside the concrete diaphragm at the end of the steel girder. The composite girder outside of the diaphragm can be designed using AASHTO LRFD design provisions.

- Moment reversal such as that which could exist in seismic design is not considered.

- It is assumed that the bottom flange is predominantly subjected to compression. Type 1 and 4 connection details can be modified for application in cases where bottom flanges are subjected to significant tension, a scenario that could exist when the number of bridge spans exceeds or equals three and when uneven span length are used. More detailed discussion of this scenario is provided in Azizinamini (2014). Type 3 connection detail is not applicable when bottom flanges are subjected to significant tension.

Continuous Bottom Flange (Type 1) and Modular (Type 4)

In this type of connection, for the case of negative flexure, the tension force is mainly resisted by longitudinal reinforcement in the slab. The compression force is resisted, predominately by bottom plate or steel block. The failure of the connection can be initiated by yielding of the bottom plate, yielding of the top rebar or crushing of the diaphragm concrete. To avoid crushing the concrete in the vicinity of the bottom plate, this plate (block) is sized to stay elastic when all reinforcement in the slab reaches its ultimate capacity, which is larger than yield capacity.

If the plate is to remain elastic until all slab reinforcement reaches its ultimate capacity, then it can be assumed that the core concrete will not crush. The net result is that the failure of the connection will coincide with slab reinforcement reaching its ultimate capacity. It should be noted that the ultimate capacity of the slab reinforcement is equal to total area of slab reinforcement multiplied by the ultimate strength of reinforcement.

Predicting the ultimate strength of the slab reinforcement could be achieved by examining the available information on material properties of the reinforcement used. For the sake of developing design provisions, it is assumed that ultimate strength of reinforcement is related to yield stress, using following relationship:

$$F_u = \alpha f_y \qquad (21)$$

where

α = ductility ratio of rebar
F_y = yield stress of deck rebar

Thus, for the compression plate to remain elastic under ultimate load, the desired height of the compression plate conservatively is

$$H > \frac{\alpha A_s f_y}{b_f F_{pl}} \qquad (22)$$

where

A_s = total area of deck reinforcement
F_{pl} = yield stress of compression plate or block

Because a large majority of the compressive force is resisted by the stiff compression plate, as evidenced by the low neutral axis, the resultant of the compressive force will be located within the compression plate. Also, because it has been assumed that the deck reinforcement is the only portion of the cross-section that can resist any tensile stress, an estimate of the moment arm, which is the distance between center of tension and compression resultant forces, is easily obtained. Under these assumptions, the moment arm

is simply distance between center of reinforcement in the top and center of steel block in the bottom. The moment capacity of the connection is then estimated using following equation:

$$M_n = A_s f_y \left(d - H/2 \right) \tag{23}$$

For comparison purposes, the nominal capacity of the first test specimen was calculated, using the measures yield strength of reinforcing bars (65.4 ksi):

$$M_n = (19.4)(65.4)(43 - 1.2/2)$$
$$= 53{,}795 \text{ kip-in.}$$

The nominal capacity just calculated is approximately 72% of the moment obtained from the experimental test (74,304 kip-in.).

For the fourth tested specimen, the capacity is:

$$M_n = (19.4)(66.5)(43.2 - 4/2)$$
$$= 53{,}152 \text{ kip-in.}$$

The nominal capacity is approximately 79% of the ultimate moment obtained from the test (67,500 kip-in.).

End Plate (Type 3)

This detail is not recommended for new design. However, it may have applicability to cases where existing bridges are retrofitted and simple spans are made continuous.

The geometry of the third specimen type bears a strong resemblance to that of simple-made-continuous prestressed concrete connections. Due to the similarity of these connections, the same method used for prestressed concrete connection as recommended by the PCI *Bridge Design Manual* (PCI, 1997) may be sufficient for the design of this connection in steel girder bridges as well. However, the additional aspect that is added to the design method pertains to the confinement of the core concrete, which increases the capacity of the connection.

In order to obtain an appropriate design method for this detail, it is clear that the confinement needs be taken into consideration. The enhanced concrete compressive strength because of confinement can be estimated using Equation 9. Using the magnified strength, it is proposed that standard reinforced concrete design methods be used.

To ensure the ductility of section, it is recommended to use AASHTO LRFD requirements, as stated by Equation 24:

$$\frac{c}{d} = 0.42 \tag{24}$$

The objective of the preceding limitation is to prevent use of sections with very large compression block. For type 3 connection details, Kowalski (2007) indicates that the c/d

ratio can be as large as 0.62 when confinement effects are considered.

To demonstrate the simple design procedure, the moment capacity of the third test specimen is calculated based on Equation 9:

$$q = 0.38\sqrt{5.9} + 5.9$$
$$= 6.82 \text{ ksi}$$

$$a = f_y A_s / (0.85 q b_f)$$
$$= (69.2)(19.4) / [0.85(6.82)(15.8)]$$
$$= 14.7 \text{ in.}$$

$$c = a/\beta$$
$$= 14.7/0.85 = 17.2 \text{ in.}$$

$$c/d = 17.2/43$$
$$= 0.4 < 0.42 \text{ ok}$$

$$M_n = A_s f_y (d - a/2)$$
$$= 19.4(69.2)(43 - 14.7/2)$$
$$= 47{,}859 \text{ kip-in.}$$

The nominal moment capacity is approximately 68% of the capacity of the tested specimen (70,380 kip-in.). One main reason for the conservative prediction of the moment capacity by the simplified equation is the overstrength of the top longitudinal rebar, which was ignored in the simplified equations. Kowalski (2007) showed that this level of conservative design is in line with current practice of cast-in-place concrete beam flexure design.

PARAMETRIC STUDIES

Two different studies were carried out to investigate the efficacy of the simplified design equations. The first study focused on the connection types 1 and 4, which rely on steel to provide continuity of the compressive force at the bottom flange. The second study considered the type 3 connections, which utilize concrete to transmit the compressive force.

Continuous Bottom Flange (Type 1) and Modular (Type 4)

To verify the validity of the proposed method, a typical 100-ft span bridge was designed according to AASHTO LRFD bridge specifications. The bridge was designed to act as a simple span for the dead loads and continuous for the live loads. The bottom plate, which connects the bottom flanges of the girders in the core region as shown in Figure 1, was considered to have five different heights, *H*.

A finite element model was constructed and analyzed to obtain the ultimate capacity of the specimen for each plate height, as listed in column 4 of Table 2. The ultimate moment capacity of the connection at the pier centerline was calculated using the detailed method described earlier and

Table 2. Ultimate Moment Capacity Comparison of Simplified and Detailed Prediction Methods versus Finite Element Results			
	M_u (kip-in.)		
H (in.)	Simplified	Detailed	FEA
0.5	45,408	53,319	57,523
1.0	45,078	57,063	61,638
1.73	44,596	63,785	69,667
2.16	44,312	61,419	72,539
4.0	43,098	62,266	74,318

Table 3. Parametric Study Variables						
		Span of Each Bridge				
Input	Units	50 ft	75 ft	100 ft	125 ft	150 ft
Steel girder flange width	in.	10.4	11.5	12.215	16.51	16.87
Concrete core thickness	in.	2	4	5	6	8
f'_c	ksi	4	4.5	5.5	6	6.5
Diaphragm thickness	in.	10	15	20	25	30
Width of the slab/diaphragm	in.	96	108	120	132	144
Slab thickness	in.	7	7	7.5	7.5	8
Total area of the slab rebar in longitudinal direction	in.^{2}	7	15	22	30	35
Yield strength of steel rebar	ksi	60	60	60	60	60

listed in the third column of Table 2. The capacity was also computed using the simplified method developed earlier and listed in the second column of Table 2.

End Plate (Type 3)

Two-span I-girder bridges were designed according to AASHTO-LRFD bridge specifications to examine the proposed design method for the type 3 connection. The bridge dimensions were selected in order to cover a practical range. The bridge properties are summarized in Table 3. The bridges consist of four equally spaced I-girders. The interior girder for each bridge is designed for the applied dead loads and HL-93 live load according to AASHTO LRFD provisions. The bridges were analyzed acting as two simple spans for the dead weight and as continuous for the superimposed dead loads and live loads. The bridges were designed for several load combinations, including constructability, strength limit state I, and service limit state II. The proposed design methods were used to evaluate the required longitudinal tensile reinforcement at the pier location in the slab. In the design of steel girders and slab rebar, several iterations were made to find an optimum section.

The designed bridges were analyzed using nonlinear

finite element analysis. The ultimate strengths of the bridges at the pier centerline were compared with what were predicted by the design methods developed in previous sections of this paper (see Table 4).

It is observed that the predicted capacity, in general, is in good agreement with FEA results. However, for the longer span, the simplified equations result in slightly higher ultimate moment capacity. In calculations presented earlier, the effective width was assumed to equal to tributary width.

CONCLUSIONS

The SDCL concept for steel bridges requires a connection between the girders over the bridge piers. In this paper, the structural behavior of four proposed connections was investigated through numerical and analytical methods. The comparison of the finite element models of the four connections exhibit good agreement with the results obtained from the full-scale tests. Based on numerical, analytical and experimental results, the force-resistance mechanisms of the connections are described in the form of mathematical equations. Good comparisons were obtained between results of nonlinear finite element analysis and a detailed approach to

Table 4. Ultimate Moment Capacity Comparison of Simplified and Detailed Prediction Methods versus Finite Element Results					
	Span of Each Bridge				
Method	50 ft	75 ft	100 ft	125 ft	150 ft
Simplified	13,247	28,930	46,179	73,056	102,409
Detailed	13,783	30,520	48,240	74,272	103,477
FEA	17,294	33,054	49,542	72,276	101,298

calculate moment capacity of all connection detail types. For practical purposes, a set of simplified equations were derived from the more detailed approach mentioned earlier for two connection types to calculate the ultimate negative moment capacity at the critical sections. The simplified approach is recommended for use in the design process.

REFERENCES

AASHTO (2007), *LRFD Bridge Design Specifications*, 4th ed., American Association of State Highway and Transportation Officials, Washington, DC.

ABAQUS (2009), *ABAQUS Theory Manual,* SIMULIA, Providence, RI.

Azizinamini, A. (2014), "Simple for Dead Load–Continuous for Live Load Steel Bridge Systems," AISC, *Engineering Journal*, Second Quarter.

Azizinamini, A., Lampe, N.J. and Yakel, A.J. (2003), *Toward Development of a Steel Bridge System—Simple for Dead Load and Continuous for Live Load*, Final Report for Nebraska Department of Roads Research Project Number SPRL-PL-1(035) P515, University of Nebraska–Lincoln, Lincoln, NE.

Azizinamini, A., Yakel, A.J., Lampe N.J., Mossahebi, N. and Otte, M. (2005), *Development of a Steel Bridge System—Simple for Dead Load and Continuous for Live Load, Volume 2: Experimental Results*, Final Report NDOR P542, Nebraska Department of Roads, Lincoln, NE.

Farimani, M.R. (2006), *Resistance Mechanism of Simple-Made-Continuous Connections in Steel Girder Bridges*, Ph.D. Dissertation, University of Nebraska–Lincoln, Lincoln, NE.

Javidi, S.N. (2009), *Resistance Mechanism of Simple-Made-Continuous Connections in Skew and Non-Skew Steel Girder Bridges Using Conventional and Accelerated Types of Construction*, Ph.D. Dissertation, University of Nebraska–Lincoln, Lincoln, NE.

Javidi, S.N., Yakel, A.J. and Azizinamini, A. (2014), "Experimental Investigation, Application and Monitoring of a Simple for Dead Load–Continuous for Live Load Connection for Accelerated Modular Steel Bridge Construction," AISC, *Engineering Journal*, Third Quarter (in press).

Kowalski, D.T. (2007), *Development and Evaluation of Design Equations for the Simple-Made-Continuous Steel Bridge System*, M.S. Thesis, University of Nebraska–Lincoln, Lincoln, NE.

Lampe, N.J. (2001), *Steel Girder Bridges Enhancing the Economy*, M.S. Thesis, University of Nebraska–Lincoln, Lincoln, NE.

Lampe, N.J., Mossahebi, N., Yakel, A.J., Farimani, M.R. and Azizinamini, A. (2014), "Development and Experimental Testing of Connections for the Simple for Dead Load–Continuous for Live Load Steel Bridge System," AISC, *Engineering Journal*, Second Quarter.

Mossahebi, N. (2004), *New Steel Bridge System: Simple for Dead Load, Continuous for Live Loads*, M.S. Thesis, University of Nebraska–Lincoln, Lincoln, NE.

PCI (1997), *Precast Prestressed Concrete Bridge Design Manual*, 2nd ed., Precast/Prestressed Concrete Institute, Chicago, IL.

Timoshenko, S. and Goodier, J. (1970), *Theory of Elasticity*, 3rd ed., McGraw-Hill, New York, NY.

William, K.J., and Warnke, E.P. (1975), "Constitutive Model for the Triaxial Behavior of Concrete," *Proc. International Association for Bridge and Structural Engineering 19*, ISMES, Bergamo, Italy.